minerals

MDPI

Article

Influencing Factors of the Brittleness of Continental Shales Containing Shell Limestone Interlayer

Yuejiao Liu [1], Fuqiang Lai [1,*], Ruyue Wang [1,2,3,4,*], Zhonghu Wu [5], Xiaoshu Zhang [1], Hao Xu [1] and Jiao Li [1]

1 Chongqing Key Laboratory of Complex Oilfield Exploration and Development, Chongqing University of Science and Technology, Chongqing 401331, China
2 State Key Laboratory of Shale Oil and Gas Enrichment Mechanisms and Efficient Development, Beijing 102206, China
3 Sinopec Key Laboratory of Shale Oil/Gas Exploration and Production Technology, Beijing 102206, China
4 Sinopec Petroleum Exploration and Production Research Institute, Beijing 102206, China
5 College of Civil Engineering, Guizhou University, Guiyang 550025, China
* Correspondence: laifq@cqust.edu.cn (F.L.); wangruyue.syky@sinopec.com (R.W.)

Abstract: Brittleness is important in the evaluation of the fracturing ability of shale reservoir and has a significant impact on shale gas exploration and development. This paper discusses the characteristics and controlling factors of brittleness of continental shale in the Da'anzhai Member of the Ziliujing Formation of Lower Jurassic age in the northeast Sichuan Basin. Continental shale lithofacies and their associations were grouped into four main rock types: clayey shale, silty shale, shell calcareous clayey shale, and silty clayey shale, characterized by the high clay content and local enrichment of carbonate minerals as a whole. Compared with the marine shale, the continental shale contained a low content of siliceous minerals, a high content of carbonate minerals, and a large number of shell limestone interlayers. Carbonate minerals play an important role in controlling the brittleness of continental shale. The shale interlayers were mainly shell limestone interlayers with a thickness of several centimeters and a large number of shell laminates with thicknesses of several millimeters were also observed. The shell laminates were mainly filled with calcite. Due to the dissolution process, a large number of bedding joints and corrosion joints were formed in the calcite shell layers. In the interlayers with a high shell content, a large number of microfractures developed. The energy consumption required for maintaining fracture expansion was lower after fracturing; the fractures greatly improved the reservoir's brittleness.

Keywords: continental shale; brittleness; mineral component; fracture; elastic parameter

check for updates

Citation: Liu, Y.; Lai, F.; Wang, R.; Wu, Z.; Zhang, X.; Xu, H.; Li, J. Influencing Factors of the Brittleness of Continental Shales Containing Shell Limestone Interlayer. *Minerals* **2023**, *13*, 460. https://doi.org/10.3390/min13040460

Academic Editor: Luca Aldega

Received: 10 February 2023
Revised: 19 March 2023
Accepted: 22 March 2023
Published: 24 March 2023

Copyright: © 2023 by the authors. Licensee MDPI, Basel, Switzerland. This article is an open access article distributed under the terms and conditions of the Creative Commons Attribution (CC BY) license (https://creativecommons.org/licenses/by/4.0/).

1. Introduction

Shale oil and gas are widely distributed around the world and the large reservoirs of shale oil and gas deeply affect the international political and economic backgrounds [1–4]. After the United States realized energy independence through the shale oil and gas revolution, China also made great achievements in shale gas exploration and development over the past five years. In 2020, the output of shale gas was nearly 2×10^{10} m^3 and the cumulative proven geological reserves of shale gas exceeded 2 trillion m^3, displaying huge potential [5–7]. In the continental basins widely distributed in China, many sets of shale series with rich organic matter have developed, and continental shale oil and gas is an important exploration field [8–12]. Recently, in the Fuling Area of northeastern Sichuan, an industrial oil and gas flow was achieved, suggesting a key breakthrough in the exploration of Jurassic continental shale oil and gas [13].

Brittleness is important in shale reservoir evaluation because it indicates the fracturing performance of shale reservoirs and largely affects shale gas exploration and development [14–16]. In the comprehensive evaluation of continental shale reservoir, brittleness is an indispensable indicator. Compared with the marine shale in North America and

China [17–21], the continental shale in China is characterized by the low content of siliceous minerals, the high content of clay minerals, complex mineral composition, strong heterogeneity of reservoirs, the thinness of single layers, significant changes of lithology and lithofacies, more developed fractures, and frequent interaction between shale and interlayers (such as sandstone and limestone) [22–26]. The evaluation system of marine shale is not applicable to continental shale [27,28], so it is necessary to explore its complexity and particularity and clarify the brittleness of continental shale. Therefore, the brittleness evaluation method of continental shale gas reservoirs is significant in the exploration of geological characteristics and enrichment mechanisms of continental shale gas as well as in the geological evaluation of continental shale gas and continental strata.

In this study, with the shale series of the Da'anzhai Member of the Lower Jurassic Ziliujing Formation in the Yuanba and Fuling Area in northeastern Sichuan as the research object, lithofacies, mineral components, dynamic and static rock mechanical properties, and diagenetic stages were explored to improve the understanding of the brittleness of continental shale reservoirs and clarify the influences of minerals, fractures, and interlayers on brittleness of continental shale. This study provides the basis for the optimization of desert sections in geological engineering of continental shale reservoirs.

2. Geological Setting

The Jurassic System is widely distributed in the Sichuan Basin and the strata are well developed. In the Early Jurassic period, a set of relatively stable shallow to semi-deep lake facies shale systems was deposited [29]. The diverse interlayers in the shale mainly included shell limestone (argillaceous) and siltstone (argillaceous). The thickness center is located in the Langzhong–Liangping–Wanzhou Area (Figure 1) [30]. The TOC content in shale ranges from 0.5% to 2.0% and the average TOC content is greater than 1%. The type of organic matter is mainly Type II2 and the vitrinite reflectance (*Ro*) gradually increases from southeast to northwest. Ro from eastern Sichuan to northeastern Sichuan is generally greater than 1.3%, indicating the condensate wet gas stage. The Yuanba and Fuling Areas are located in the northeast of the Sichuan Basin. The Yuanba Region is located at the junction between the depression structure in the western Sichuan area and the uplift structure in central Sichuan. The Fuling Area is located in the high and steep fold belt in eastern Sichuan.

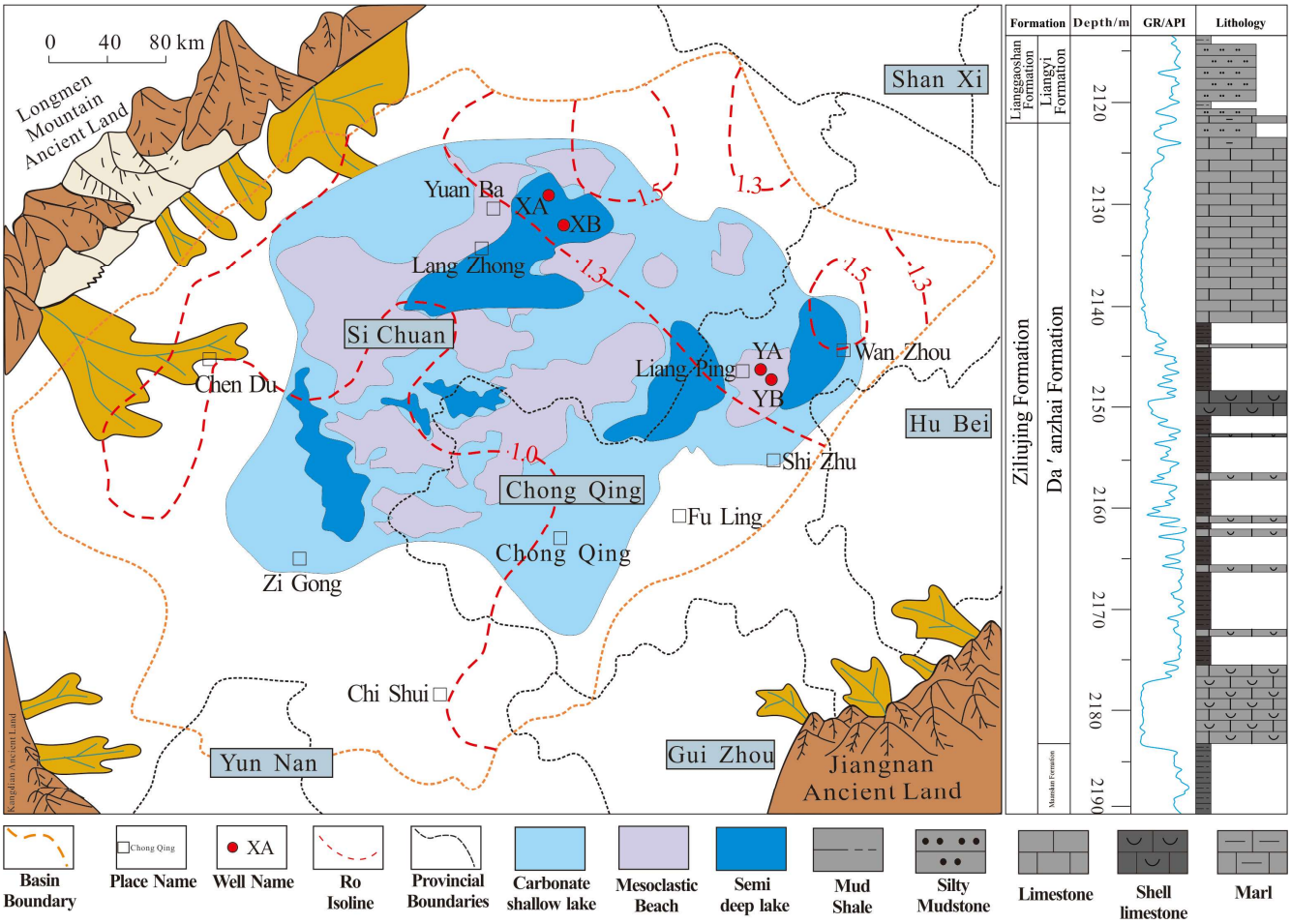

Figure 1. Sedimentary and distribution characteristics of the Jurassic Ziliujing Formation in the Sichuan Basin.

3. Samples and Methods

The core and logging data in this study were collected from the continental shale sequence in the Yuanba and Fuling Areas in the Sichuan Basin, China. Forty-six small core samples with a length of about 50 mm and a width of about 25 mm were drilled from the core. The logging data included conventional logging, array acoustic logging, element logging (ECS), and electrical imaging logging data.

The samples were subjected to the analysis of organic carbon content, identification of organic macerals, determination of helium porosity and permeability, whole-rock mineral analysis, argon ion polishing–scanning electron microscope analysis, pore structure analysis, rock pyrolysis experiments (including field analysis), and a triaxial rock mechanics experiment. The TOC test was conducted in the carbon and sulfur analyzer CS-230 according to GB/T 19145-2003. The reflectance of vitrinite was measured using the MSP200 microphotometer according to the SY/T 5124-2012 standard. The whole rock mineral X-ray diffraction (XRD) analysis was carried out according to the SY/T6210-1996 standard with an X'Pert Pro MPD X-ray diffractometer at Wuxi Institute of Petroleum Geology, Wuxi, China. Porosity and permeability were measured, respectively, with a KX-07F porosity instrument and a GDS-90F permeability instrument according to the GB/T 29172-2012 standard. Argon ion polishing–scanning electron microscope observation was carried out with the Helios 650 scanning electron microscope according to the SY/T 5162-2014 standard at Wuxi Institute of Petroleum Geology, Wuxi, China. The pore structure was determined using the mercury porosimetry adsorption method according to the NB/T 14008-2015 standard. Rock pyrolysis was determined with a Rock-EVAL6 instrument according to the

GB/T 18602-2012 rock pyrolysis analysis method at Wuxi Institute of Petroleum Geology, Wuxi, China. The triaxial compressive strength test of rock mechanics was conducted with a TAW-2000 electro-hydraulic servo rock mechanics tester according to the ASTM D2664-04 standard at Wuxi Institute of Petroleum Geology, Wuxi, China. The interpretation of conventional logging data, array acoustic logging data, FMI resistivity imaging logging data, and element logging data was conducted on the large logging processing and interpretation software platform CIFLOG Version 2.1 developed by the Institute of Logging and Remote Sensing Technology of the China Petroleum Exploration and Development Research Institute.

4. Results and Discussion

4.1. Lithofacies and Mineral Fabric Characteristics

4.1.1. Lithofacies Characteristics

The fine identification and classification of continental shale lithofacies types is an important basis for the evaluation of shale gas exploration and development potential. In the previous studies on this area, the main factors considered in the lithofacies classification scheme of Daanzhai Section were mineral fabric, TOC, and sedimentary structure. According to the report by Liu Zhongbao et al. [24], the three-step lithofacies division scheme (Figure 2) of whole-rock mineral partition, TOC classification, and correction of mineral and sedimentary structures was adopted in the study (I is a muddy (shale) rock area, II is a mixed rock area, III is a sandstone area, and IV is a limestone (dolomite) rock area). Based on the observations and descriptions of the cores of four typical drilling wells in the Yuanba Area (Well XA and Well XB), Fuling Area (Well YA and Well YB), the whole-rock mineral X-ray diffraction analysis, and rock slice identification analysis of 46 samples, 4 shale types (10 shale lithofacies) were determined as follows: clayey shale (high-carbon, medium-carbon, and rich-carbon clayey shale), silty shale (low-carbon, medium-carbon, high-carbon, and rich-carbon silty shale), clayey shell calcareous shale (medium-carbon and high-carbon clayey shell calcareous shale), and silty clay shale (low-carbon and medium-carbon silty clay shale). A large number of shell limestone interlayers in the lithofacies were observed. Among them, high-carbon clayey shale (TOC: 0.59%~3.89%; average: 1.46%) and low-to-medium-carbon silty sand shale were the most common shales (TOC: 0.20%~1.60%, average: 0.89%), followed by high-carbon clayey shell calcareous shale (TOC: 0.45%~3.06%, average: 1.29%) (Figure 3).

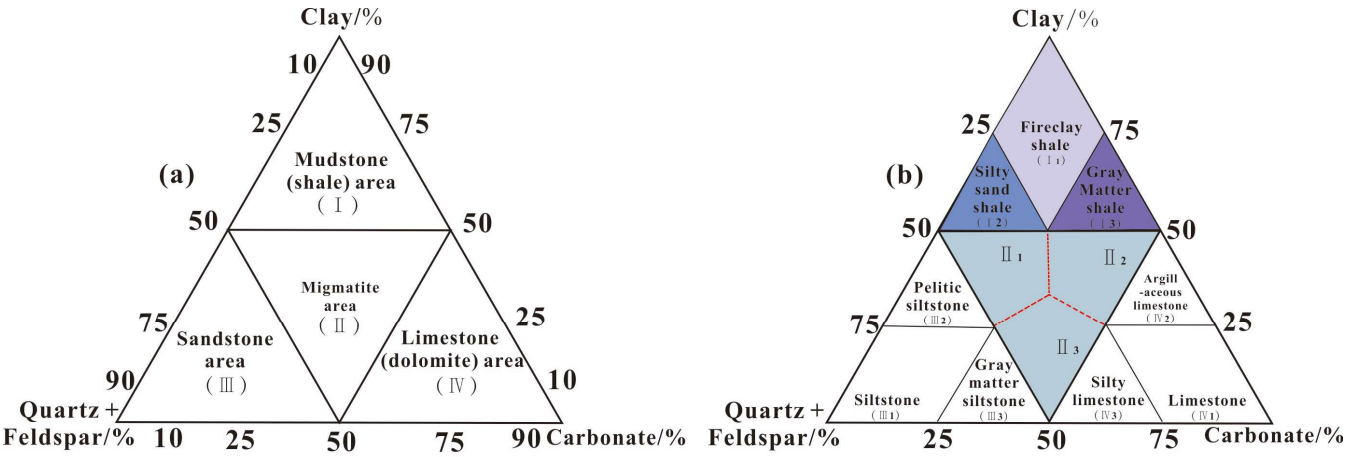

Figure 2. *Cont.*

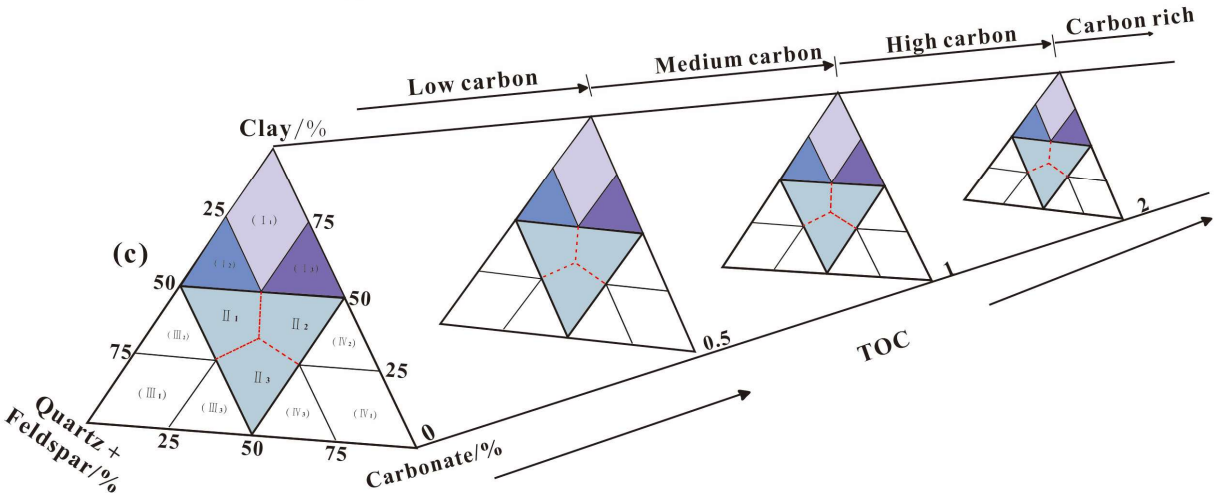

Figure 2. Lithofacies Division Scheme (revised from the method by Liu Zhongbao et al. [24]).

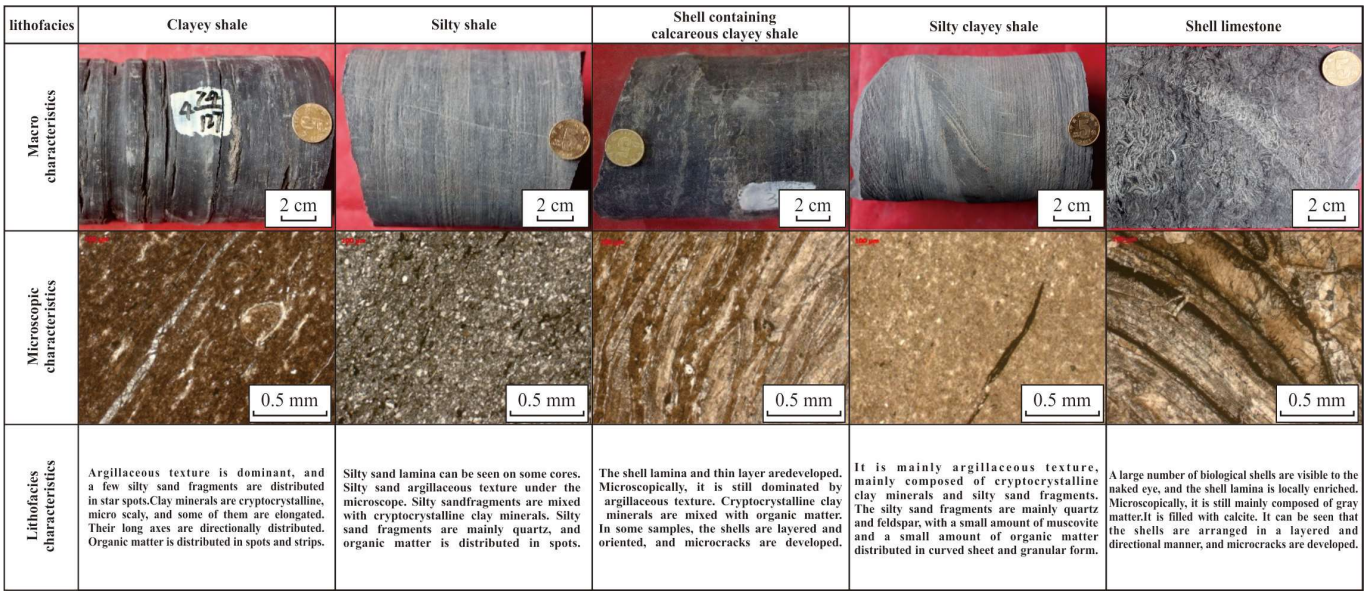

Figure 3. Main lithofacies types of shale in the Da'anzhai Member.

In the Fuling Area, the shale lithofacies were dominated by medium- and high-carbon clayey shale, followed by high-carbon clayey calcareous shale (Figure 4a–c). The shale lithofacies in the Yuanba Area were mainly composed of medium- and high-carbon clayey shale and mixed shale (Figure 4d–f).

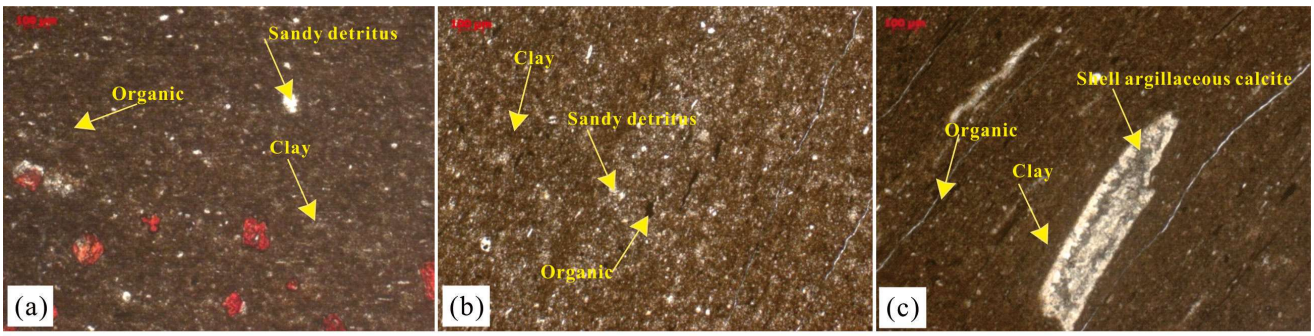

Figure 4. *Cont.*

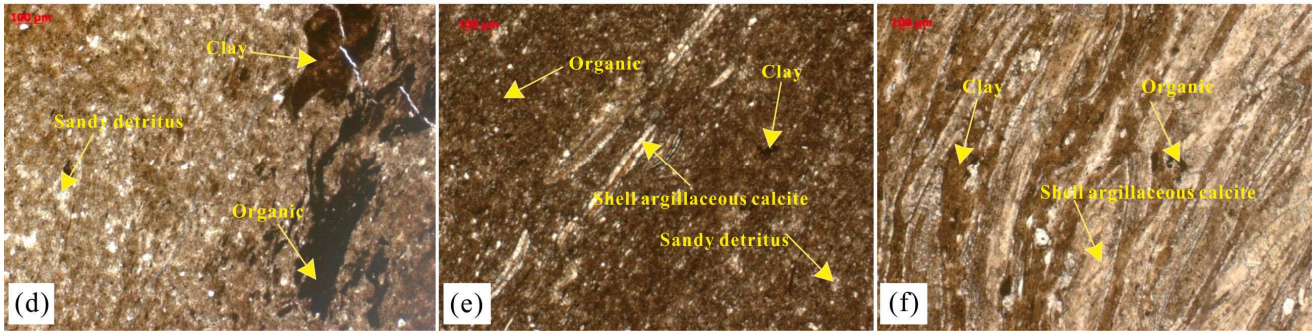

Figure 4. Microscopic photos of continental shale: (**a**) High-carbon clayey shale. (**b**) Medium-carbon calcareous clayey shale. (**c**) Medium-carbon clayey shale. (**d**) Medium-carbon clayey shale. (**e**) Medium-carbon clayey shale. (**f**) Medium-carbon clayey shell calcareous shale.

4.1.2. Mineral Fabric Characteristics

The ECS element logging data (Figure 5a) and the results of the whole-rock mineral X-ray diffraction analysis (Figure 5b) showed that the mineral components of continental shale in the Yuanba Area mainly included clay minerals and quartz, followed by calcite and a small quantity of feldspar and mica. The clay mineral content (n = 46) ranged from 21.54% to 68.3% with an average of 48.29%. The total content of quartz and feldspar ranged from 17.1% to 60.3% with an average of 35.69%. The carbonate mineral content ranged from 0 to 48.8% with an average of 12.57%. In general, the contents of clay mineral and quartz were high and carbonate minerals were locally enriched. Continental shale in the Yuanba and Fuling Areas was deposited in shallow and semi-deep lake environments of carbonate rocks (Figure 1). Compared with the marine shale of the Wufeng Formation–Longmaxi Formation (Figure 6a), the continental shale of the Da'anzhai Member had the lower content of siliceous minerals and the highest content of carbonate minerals (Figure 6b). The drilling data and rock slice identification results indicated that the enrichment of carbonate minerals in the continental shale layer was ascribed to the existence of a large number of local shell limestone interlayers. The minerals in the shell limestone mainly included argillaceous calcite, bright calcite, argillaceous, and a large number of developed microfractures (Figure 7).

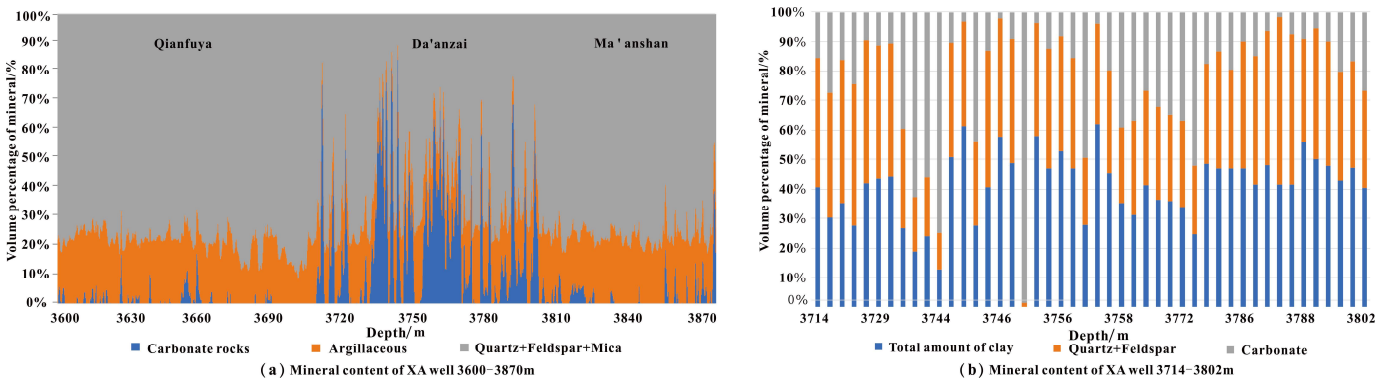

Figure 5. Mineral composition characteristics of the whole rock. (**a**) The ECS element logging data of XA well 3600–3870 m. (**b**) The whole-rock mineral X-ray diffraction analysis of XA well 3714–3802 m.

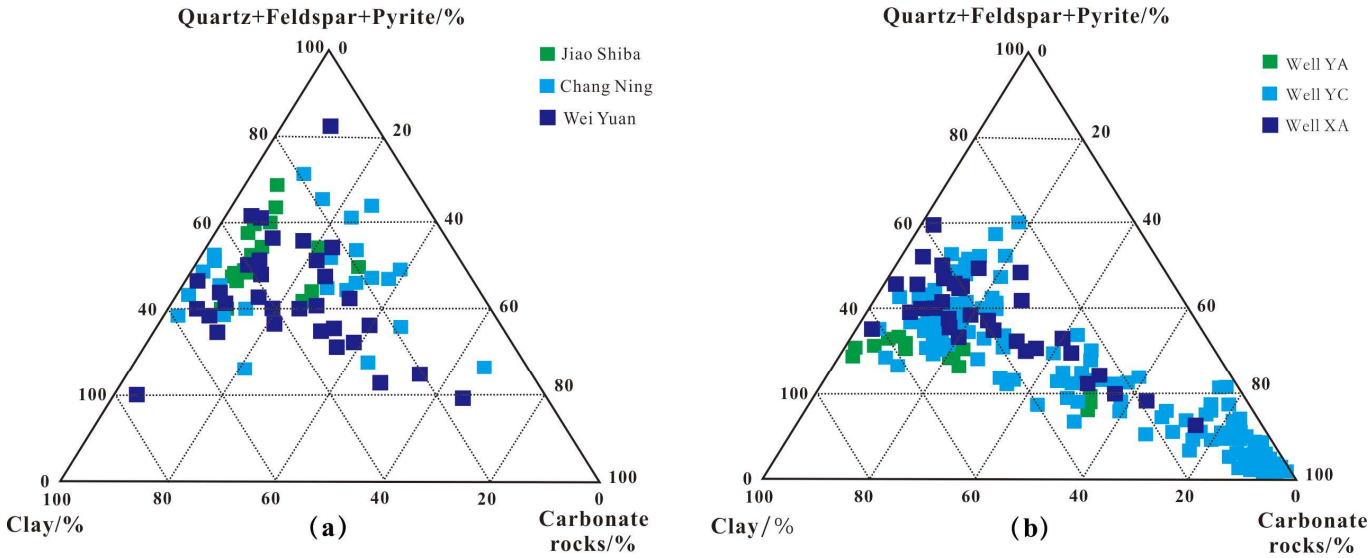

Figure 6. Comparison Diagram of Mineral Composition of Wufeng Formation–Longmaxi Formation Marine Shale and Da'anzhai Member Continental Shale: (**a**) Wufeng Formation–Longmaxi Formation, (**b**) Da'anzhai Member.

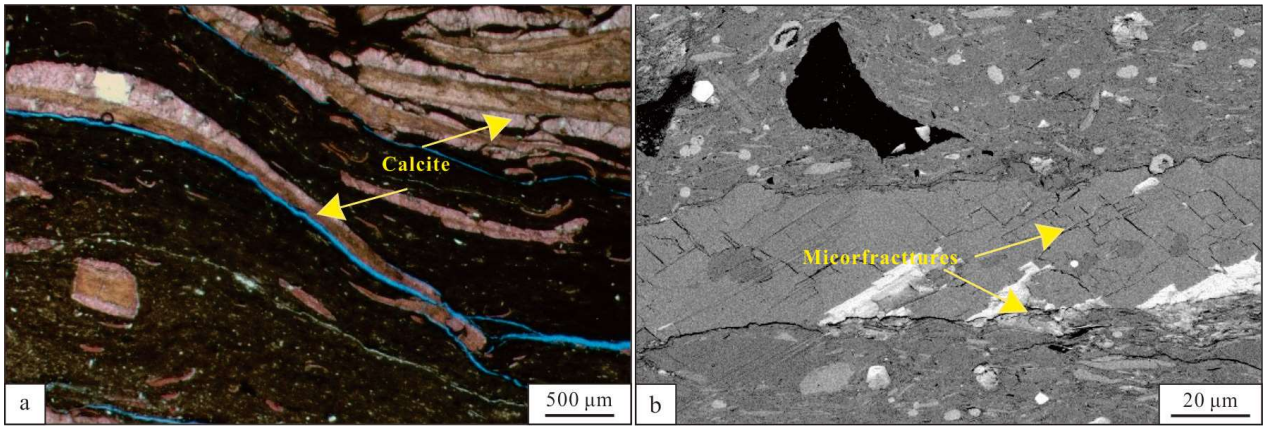

Figure 7. Characteristics of microfractures in the shell limestone interlayer. (**a**) A large amount of calcite in the shell. (**b**) A large number of microfractures develop in the shell.

The continental shale series were deposited in shallow and semi-deep lake environments of carbonate rocks. Compared with the marine shale of the Wufeng Formation–Longmaxi Formation, continental shale is characterized by the lower content of siliceous minerals, higher content of carbonate minerals, frequent interlayers, and strong heterogeneity. Therefore, the evaluation of continental shale brittleness needs to focus on the influences of the contents and distributions of carbonate minerals as well as shell limestone interlayers on brittleness.

4.2. Characteristics and Influencing Factors of Shale Brittleness

4.2.1. Mineral Content

The brittleness of continental shale was affected by mineral content and mineral structure. The dynamic and static rock mechanical parameters of continental shale in Well XA and their relationships with mineral content were analyzed with array acoustic wave and ECS logging results. The content of felsic minerals showed a negative correlation with Young's modulus, whereas the content of carbonate minerals had a positive correlation with Young's modulus (Figure 8a,b). The results of the continental shale were the opposite of the positive correlation between quartz and Young's modulus of southern marine shale [31] and

similar to that of the marine shale of the first member of the Shahejie Formation in Bonan Sag, Bohai Bay Basin [32]. In addition, the content of felsic and carbonate minerals had a good positive correlation with Young's modulus (Figure 8c), indicating that the brittleness of shale series rocks was mainly determined by the total content of carbonate and felsic minerals. Therefore, the mineral brittleness index method based on mineral composition and the elastic parameter method based on Young's modulus and Poisson's ratio [33,34] were used to calculate the brittleness index Brit1 (felsic and carbonate minerals) and the rock mechanical brittleness index Brit2 (average mechanical parameter) of continental shale and analyze their relationships. The analysis results showed that the mechanical brittleness index was correlated with the brittleness index of felsic and carbonate minerals (Figure 8d).

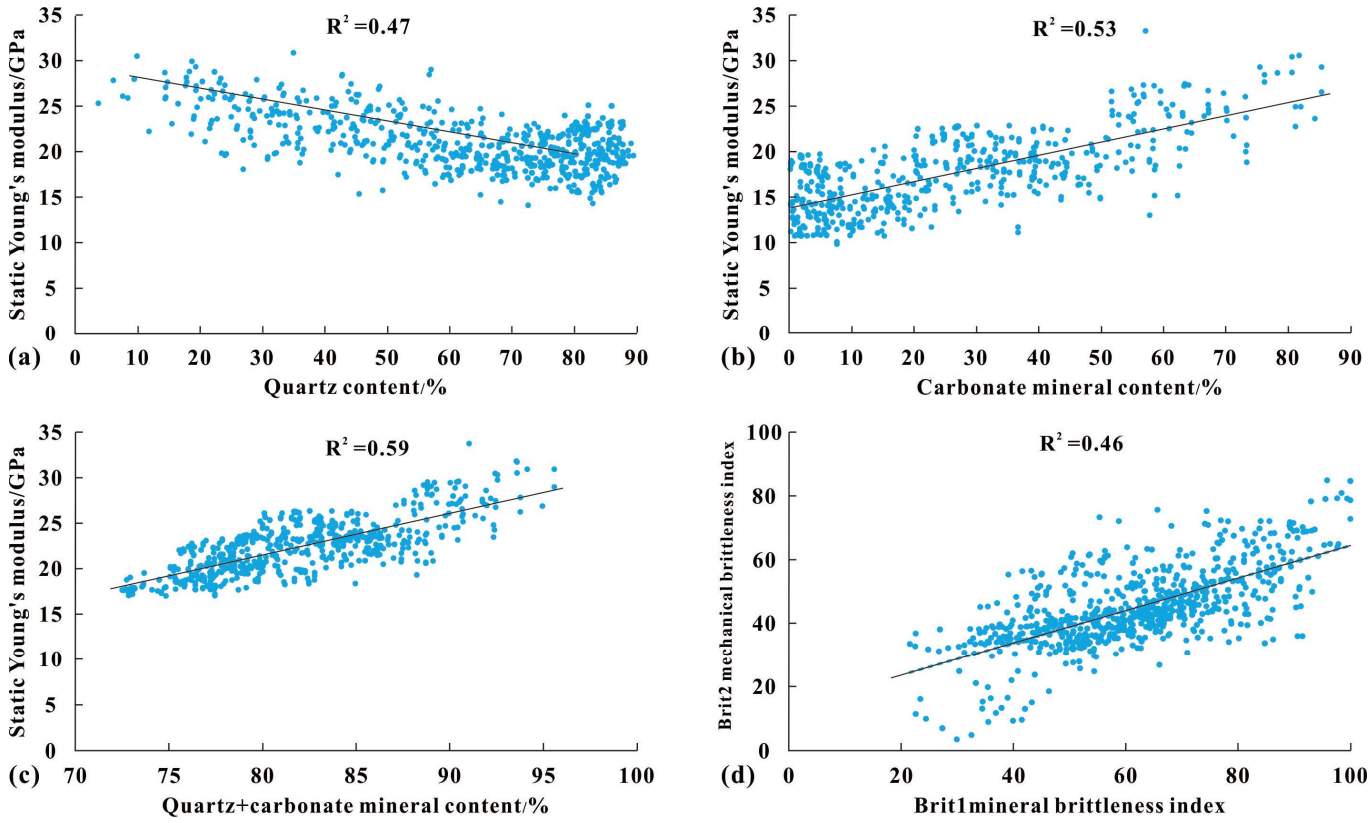

Figure 8. Relationship between rock mineral composition and mechanical parameters. (**a**) Relationship between quartz content and Young's modulus. (**b**) Relationship between carbonate content and Young's modulus. (**c**) Relationship between quartz + carbonate content and Young's modulus. (**d**) Relationship between mineral brittleness index and mechanical brittleness index.

4.2.2. Fractures

According to the previous results [35], the main component of continental shell was calcite (Figure 9). In the early diagenetic stage of continental shale, some aragonite shells were dissolved and precipitated at the edge of aragonite to form the first generation of iron-free calcite cement. In the late diagenesis, rocks were dissolved and the dissolved pores or corrosion fractures were produced in calcite and could be filled with clay minerals, organic matter, or the second generation of iron calcite cement. In addition, the muddy calcite in the shell formed a large number of fine crystals or columnar calcite under recrystallization action.

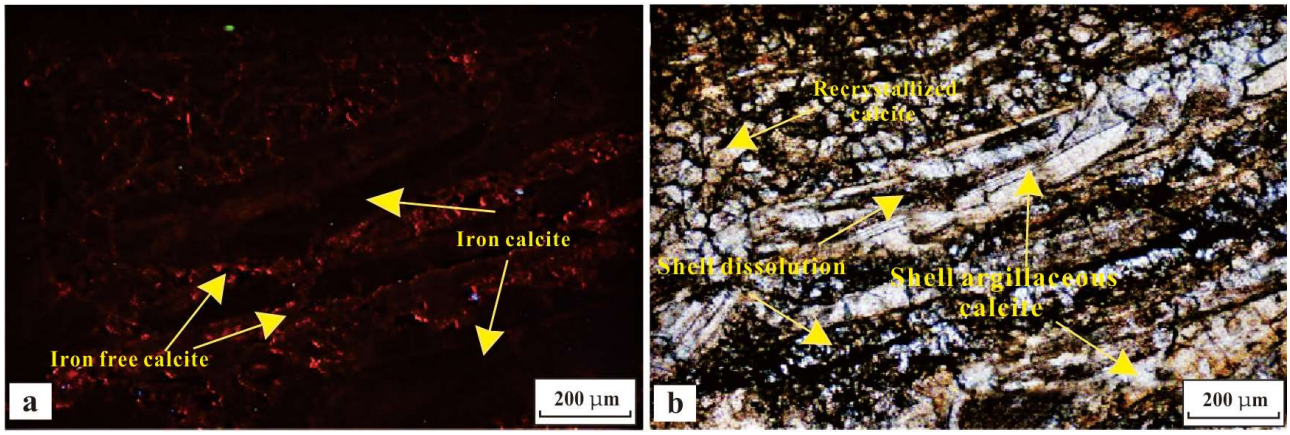

Figure 9. Calcite cement in shell [35]. (**a**) Iron-free calcite cement. (**b**) Dissolution and recrystallization of calcite.

Fracture development affected the size and anisotropy of rock mechanical parameters [36,37] and the development of a large number of calcite bedding fractures. Dissolution fractures in the whole continental shale played an important role in brittleness. The chemical properties of calcite were unstable. During the whole diagenetic stage of the Da'anzhai Member, calcite experienced multiple stages and types of diagenesis actions, including dissolution, compaction, cementation, and recrystallization. Dissolution occurred in various diagenetic stages. In the syngenetic and early diagenetic stages, atmospheric fresh water could selectively dissolve the unstable components in dissolved rocks, such as aragonite, to form dissolved pores. In the late diagenetic stage, calcite was unselectively dissolved to form dissolved pores and fractures. The dissolution of calcite in the whole diagenetic stage was beneficial to fracture development. After dissolution, the calcite-rich shell layer formed a large number of bedding fractures and solution fractures (Figure 10), not only provided a seepage channel for the flow of shale oil and gas, but also greatly improved the brittleness and physical properties of the reservoir.

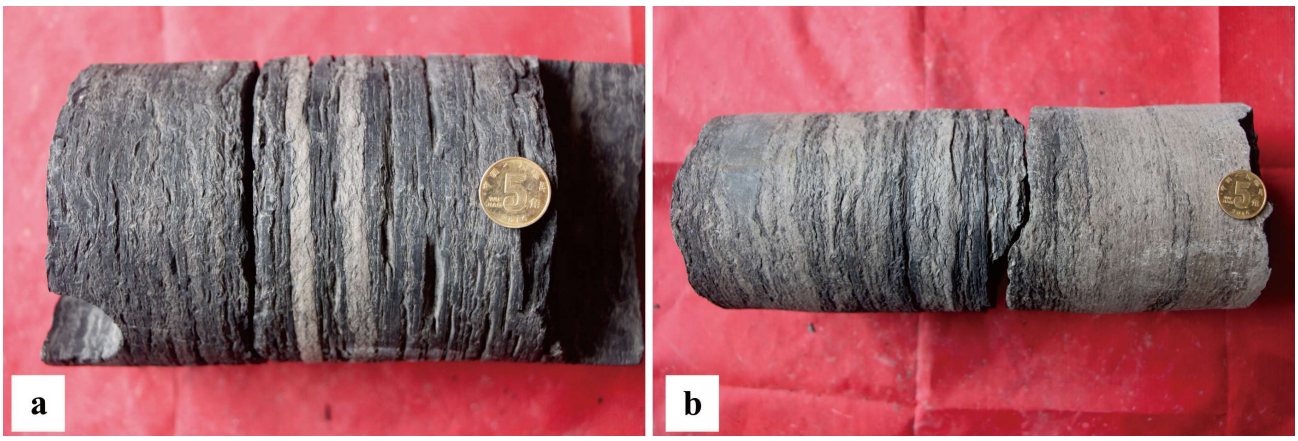

Figure 10. Coring photos with bedding fractures and dissolution fractures: (**a**) Shell mudstone has developed intermediate shell and rich bedding fractures. (**b**) Shell limestone–mudstone interbedding with developed dissolution fractures and bedding joints.

4.2.3. Shell Interlayers and Lamina

On the basis of the identification results of shale lithofacies, interlayer lithofacies, and the analysis results of lithologic profiles of typical drilling (logging) wells in different regions, continental shale of Well XA was divided into medium-carbon silty shale with argillaceous shell limestone, high-carbon clayey shale and clayey calcareous shale with argillaceous shell limestone, and low-to-medium-carbon silty shale with argillaceous shell

limestone and calcareous siltstone from bottom to top. The number of macro-scale shell limestone interlayers (meter scale) reached 14 layers/94 m. Through the fine observations and descriptions of cores in continental shale of the Well XA Member from Well XA and the rock slice identification of shale samples, the large set of shale sections in the above macro-scale lithofacies combination were observed to acquire the fine descriptions of the micro-scale (1 mm to 1 cm) lithofacies combination. A large number of millimeter-to-centimeter-scale shell calcareous laminae or bands were still developed in the single-layer continuous shale in the macro-scale lithofacies combination. In the two coring cycles of continental shale of the artesian well group of Well XA, more calcareous shell laminates were also developed in clayey shale, clayey calcareous shale, and silty shale to varying degrees, and the number of shell limestone interlayers reached 19 layers/5 m in clayey shale (Figure 11). Shell interlayers played an important role in the brittleness of clayey shale.

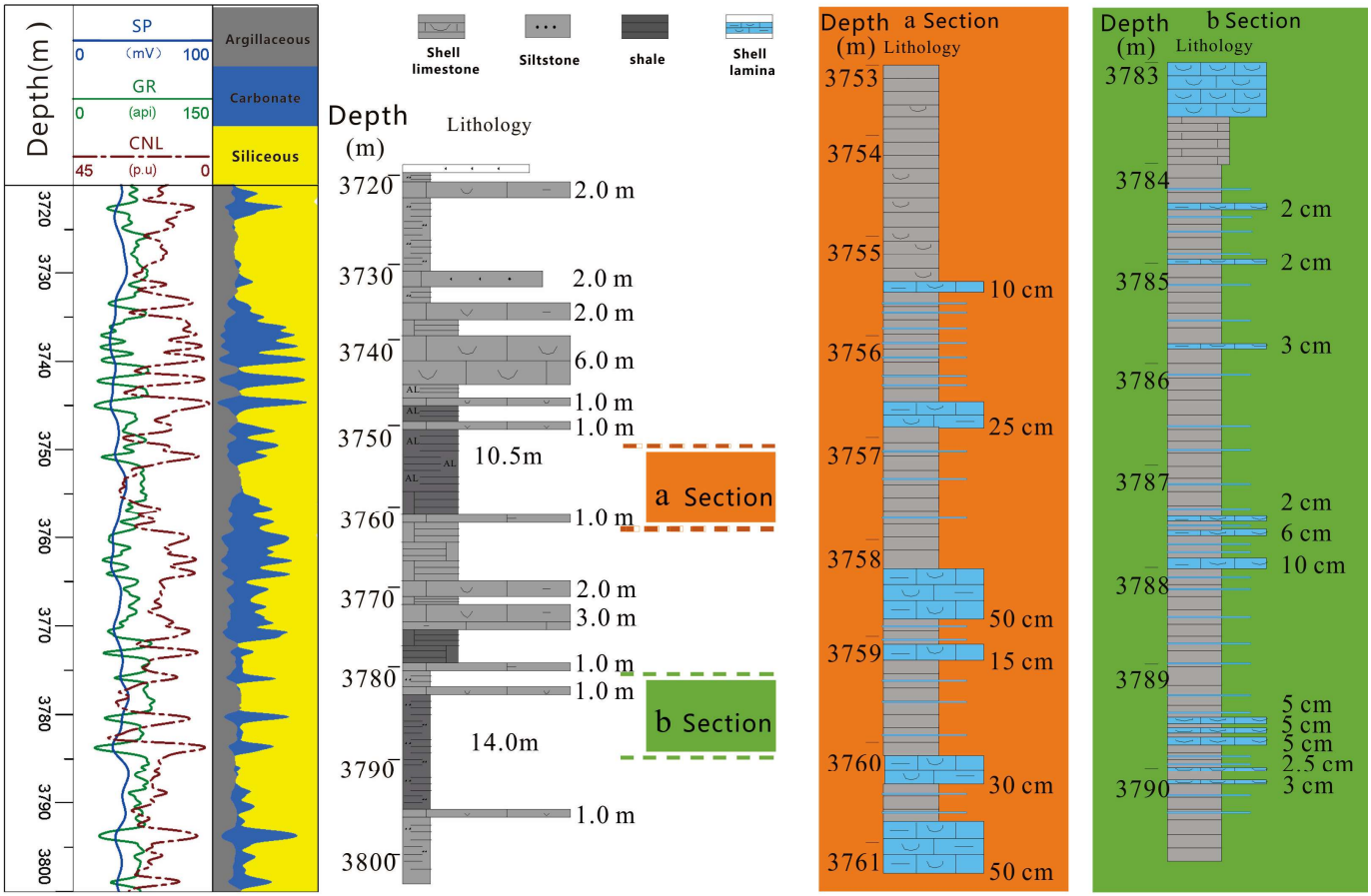

Figure 11. Lithofacies combination characteristics of continental shale in Well XA.

In order to more intuitively display the influences of shell interlayers (lamina) on reservoir brittleness, based on FMI borehole wall micro-resistivity imaging data, conventional logging curves, and logging data, different rock types and interlayers in continental shale were identified. The FMI borehole wall micro-resistivity logging tool was equipped with 192 microelectrodes on 8 plates. Each electrode had a diameter of 0.2 inches and an electrode spacing of 0.1 inches. The vertical and horizontal (around the borehole wall) resolution of the obtained electric imaging image was 0.2 inches (5 mm) [38], which was enough to identify the grain size and shape of fine conglomerates. The strata of continental shale mainly included grayish black mudstone and grayish black shale interbedded with grayish brown shell limestone layer. The corresponding electrical imaging lithological characteristics are summarized below (Figure 12). The conventional curve characteristics of mudstone were similar to those of shale. The electrical imaging results were brownish black to dark black with block characteristics and layered characteristics. Shale had a

high natural gamma radioactivity level, high neutron flux value, and low resistivity. Its electrical imaging results were brownish black to dark black with layered structures. The conventional curve of limestone was characterized by the low natural gamma radioactivity level, high density, and extremely high resistivity. The electrical imaging results were bright yellow to white with layered and massive sedimentary structures.

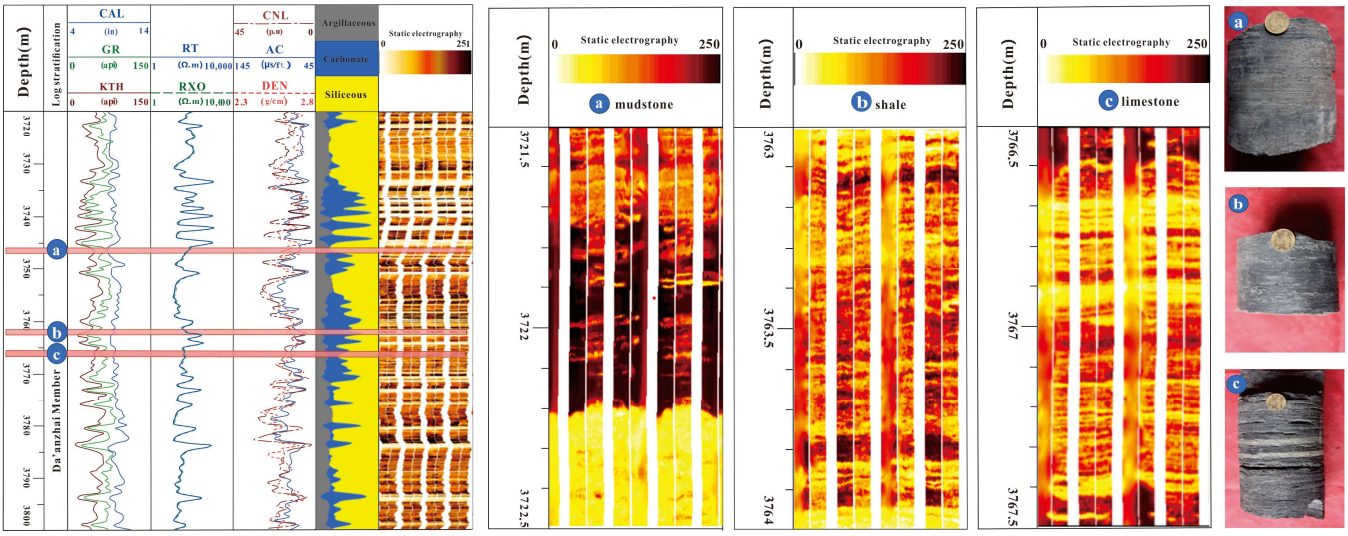

Figure 12. FMI electrical imaging characteristics of Well XA. (**a**) Electrical imaging characteristics of mudstone. (**b**) Electrical imaging characteristics of shale. (**c**) Electrical imaging characteristics of limestone.

Shale samples with low and high shell contents in the study area (Figure 13) were selected for triaxial compression tests. The stress–strain curve showed that the samples with high shell content had multiple peaks and local serration characteristics compared with the samples with low shell content. The ultimate compressive strength and residual strength were lower and the slope of the post-peak elastic modulus was steeper (Figure 14d–f), indicating that the samples with the higher shell content required lower energy to fracture and maintain fracture expansion after fracturing [36]. Therefore, the increase in shell content was more conducive to reservoir reconstruction. Through slice observations, it was found that the curve characteristics might be ascribed to a large number of microfractures developed in the shell interlayers (lamina) (Figure 7). Therefore, compared with the content of felsic minerals, the content of calcareous played the more important role in controlling the brittleness of continental shale.

The above descriptions indicated that a large number of shell interlayers (lamina) were developed in the whole continental shale. Due to the development of a large number of microfractures, the stress–strain curve of the interlayer section with a large number of shell interlayers (lamina) or a high shell content generally showed the characteristics of multiple peaks and local serration. The extreme compressive strength and residual strength were low. The slope of the post-peak elastic modulus was steep and the energy consumption required for maintaining the fracture development was lower. Therefore, compared with the content of felsic minerals, the content of calcareous played the more important role in controlling the brittleness of continental shale.

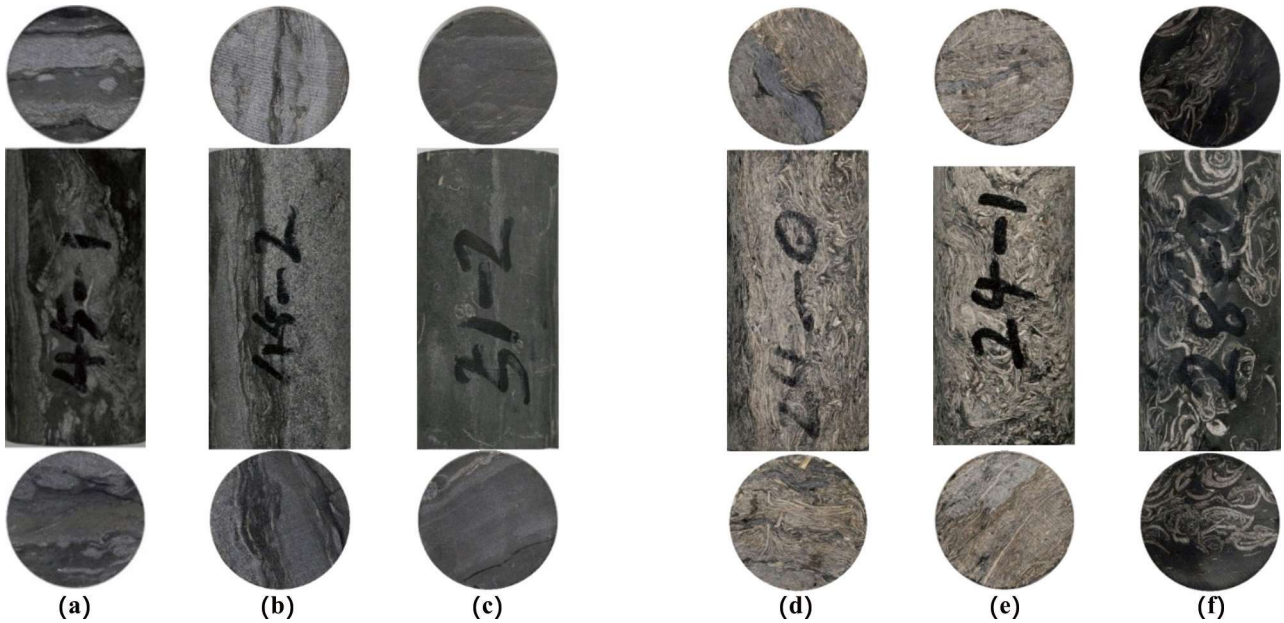

Figure 13. Shale samples with different shell contents. (**a**–**c**) Low shell content. (**d**–**f**) High shell content.

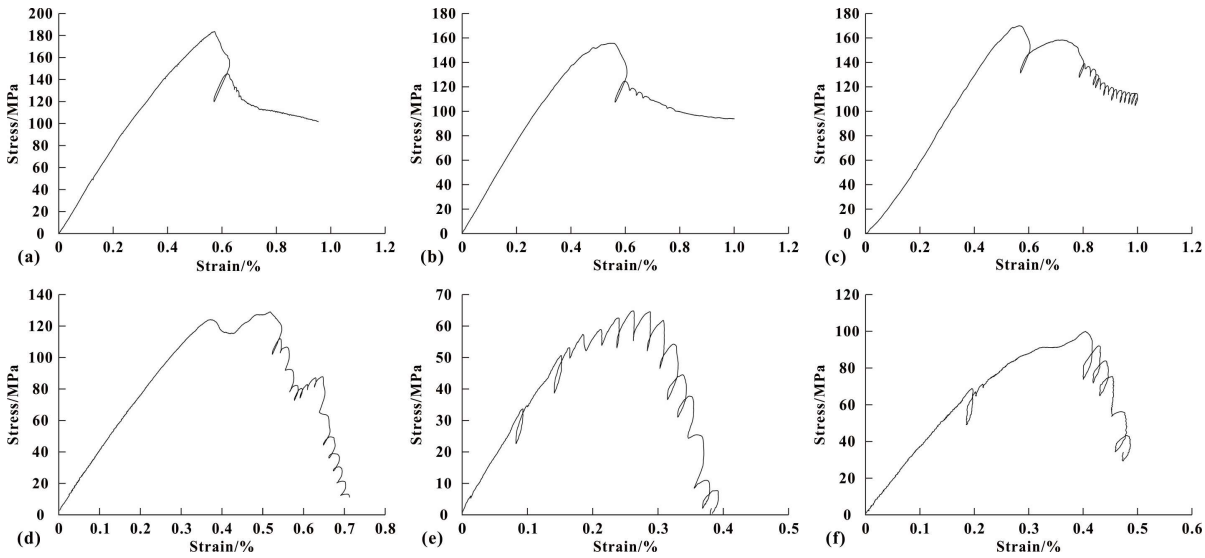

Figure 14. Stress–strain curves with different shell content. (**a**–**c**) Low shell content. (**d**–**f**) High shell content.

4.3. Actual Case Analysis

The mineral brittleness index simulation results and mechanical brittleness index model calculation results for Well XA in this study are shown in Figure 15, including mineral brittleness index Brit1 (calcite, quartz, and dolomite), average brittleness index Brit2 of mechanical parameters, quotient Brit3 of mechanical parameters, and comprehensive brittleness index Brit4 (average of Brit1 and Brit3). Compared with the brittleness index obtained from mechanical experiments, Experimental Brit (1/2 of the sum of mechanical parameters after standardization), Brit1 was relatively small and showed an insignificant brittleness change, so it was unable to accurately indicate the position of the high brittleness development stage. Brit2 was similar to Brit1 and showed the smallest overall brittleness. Brit3 was the largest brittleness index and showed a significant brittleness change. However, due to the complex stress conditions of the reservoir in the study area, the applicability

of the results remain to be verified. Brit4 comprehensively considered the influences of mineral and mechanical parameters. Compared with the first three brittleness indexes, Brit4 was highly correlated with Experimental Brit, indicating that this evaluation method was the most reasonable.

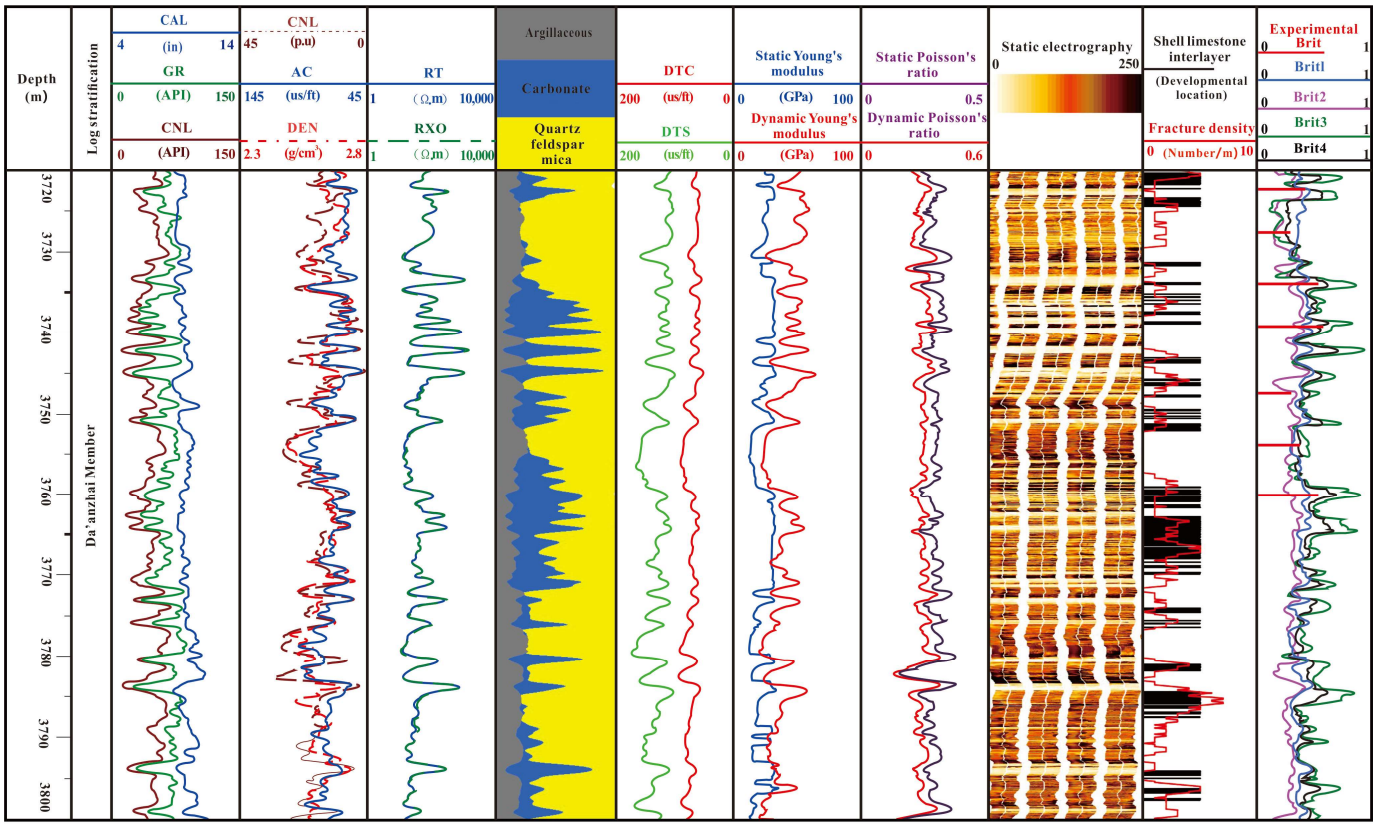

Figure 15. Calculation of brittleness indexes of Well XA.

The location of shell interlayers (lamina) and the density of the fractures of continental shale in the Da'anzhai Member were identified, and the development depth was calculated (the second track from the right in Figure 15). With the increase in the number of developed interlayers (lamina) and the fracture density, the reservoir brittleness increased significantly. Therefore, in the calculation of the brittleness index, the lamina and fractures should be quantified and comprehensively considered.

The above analysis showed that individual brittle minerals or mechanical parameters could not accurately represent the brittleness of a continental shale reservoir. The factors such as shell interlayers (lamina) and fracture development should be comprehensively considered for developing an applicable evaluation system of the brittleness and fracturing of continental shale.

5. Conclusions

(1) The continental shale lithofacies and their association types included four main rock types: clay shale, silty shale, shell calcareous clay shale, and silty clay shale, which were characterized by the high clay content and local enrichment of carbonate minerals.

(2) The brittleness of continental shale was affected by mineral content and mineral structure. The continental shale in the Da'anzhai Member was deposited in shallow and semi-deep lake environments of carbonate rocks. Compared with the marine shale of the Wufeng Formation–Longmaxi Formation, the continental shale had a lower content of siliceous minerals and higher content of carbonate minerals. The

content of felsic minerals showed a weak influence on brittleness. The total content of felsic and carbonate minerals largely determined the brittleness of shale.

(3) The continental shale contained a large number of shell laminates. The shell was mainly filled with calcite. After dissolution, the calcite shell formed a large number of bedding joints and corrosion joints. In the interlayers with a high shell content, a large number of microfractures also developed.

(4) A large number of fractures developed in continental shale, making the energy consumption required for maintaining fracture expansion after rock fracture and fracturing lower, thus greatly improving the brittleness of the shale reservoir.

(5) The main control factors for the brittleness of continental shale and marine shale are not consistent. Therefore, the lithology, interlayer type, shell content, and rock mechanical properties should be fully considered in the establishment of the corresponding brittleness and fracturing evaluation system of continental shale.

Author Contributions: Conceptualization, Y.L. and R.W.; methodology, Y.L.; software, H.X. and Y.L.; validation, J.L. and X.Z.; formal analysis, Y.L. and F.L.; investigation, Z.W. and Y.L.; resources, X.Z.; data curation, R.W.; writing—original draft preparation, Y.L. and R.W.; writing—review and editing, F.L. and Z.W.; visualization, Y.L., F.L. and R.W.; supervision, Y.L. and R.W.; project administration, F.L. and R.W.; funding acquisition, Y.L., F.L. and R.W. All authors have read and agreed to the published version of the manuscript.

Funding: This research was jointly supported by the National Natural Science Foundation of China (41402118519640075210408 0), Chongqing Basic Research and Frontier Exploration Projects (cstc2018jcyjAX0503), Chongqing Postgraduate Research and Innovative Projects (CYS22722), and Guizhou Science and Technological Supporting Plan Project (2021-401).

Data Availability Statement: Not applicable.

Acknowledgments: Thank you Sinopec Petroleum Exploration and Production Research Institute, Beijing 102206, China, for the assistance and support, and I would like to express my heartfelt gratitude.

Conflicts of Interest: The authors declare no conflict of interest.

References

1. Zou, C.N.; Yang, Z.; Dong, D.Z.; Zhao, Q.; Chen, Z.H.; Feng, Y.L.; Li, J.R.; Wang, X.N. Formation, Distribution and Prospect of Unconventional Hydrocarbons in Source Rock Strata in China. *J. Earth Sci.* **2022**, *47*, 1517–1533.
2. Adeyilola, A.; Zakharova, N.; Liu, K.Q.; Gentzis, T.; Carvajal-Ortiz, H.; Ocubalidet, S.; Harrison, W.B. Hydrocarbon potential and Organofacies of the Devonian Antrim Shale, Michigan Basin. *Int. J. Coal Geol.* **2022**, *249*, 1039509. [CrossRef]
3. Paul, D.; Malik, S.; Mishra, D.K.; Hiwale, R. Shale gas: An indian market perspective. *Int. J. Energy Econ. Policy* **2021**, *11*, 126–136. [CrossRef]
4. Cudjoe, S.E.; Barati, G.R.; Goldstein, R.H.; Tsau, J.S.; Nicoud, B.; Bradford, K.; Baldwin, A.; Mohrbacher, D. An integrated workflow to characterize lower Eagle Ford shale for hydrocarbon gas huff-n-puff simulation. *Fuel* **2021**, *289*, 119854. [CrossRef]
5. Dou, L.R.; Wen, Z.X.; Wang, J.J.; Wang, Z.M.; He, Z.J.; Liu, X.B.; Zhang, N.N. Analysis of the world oil and gas exploration situation in 2021. *Pet. Explor. Dev.* **2022**, *49*, 1195–1209. [CrossRef]
6. Davis, L.A. The Shale Oil and Gas Revolution. *Engineering* **2018**, *4*, 438–439. [CrossRef]
7. Satyavani, N.; Uma, V.; Pavan, K.P.; Srinivas, K.N.S.S.S.; Mysaiah, D.; Dhanam, K.; Srinivas, G.S.; Satyanarayana, H.V.S.; Vedanti, N. Geophysical Exploration of Unconventional Hydrocarbons. *J. Geol. Soc. India* **2021**, *97*, 1274–1279. [CrossRef]
8. Zhang, S.M.; Yang, Y.M.; Hong, H.T.; Zeng, J.H.; Zhang, R.; Li, Y.C.; He, X.Q. Reservoir characteristics and its petroleum significance of Jurassic Da anzhai shale interval in central Sichuan Basin, SW China. *J. China Univ. Min. Technol.* **2022**, *51*, 718–730.
9. Wang, R.Y.; Hu, Z.Q.; Liu, J.S.; Wang, X.H.; Gong, D.J.; Yang, T. Comparative analysis of characteristics and controlling factors of fractures in marine and continental shales: A case study of the Lower Cambrian in Cengong area, northern Guizhou Province. *Oil Gas Geol.* **2018**, *39*, 631–640.
10. Pu, B.L.; Wang, F.Q.; Dong, D.Z.; Sun, J.B. Challenges of terrestrial shale gas exploration and development from Chang 7 shale in the Ordos Basin. *Arab. J. Geosci.* **2021**, *14*, 644. [CrossRef]
11. Liu, B.; Shi, J.X.; Fu, X.F.; Lv, Y.F.; Sun, X.D.; Gong, L.; Bai, Y.F. Petrological characteristics and shale oil enrichment of lacustrine fine-grained sedimentary system: A case study of organic-rich shale in first member of Cretaceous Qingshankou Formation in Gulong Sag, Songliao Basin, NE China. *Pet. Explor. Dev.* **2018**, *45*, 828–838. [CrossRef]
12. He, J.H.; Ding, W.L.; Li, R.N.; Wang, R.Y.; Zhao, W. Forming condition of the continental shale gas of Shaheji Formation in the central-north Huanghua depression and its resource prospect. *Pet. Geol. Recovery Effic.* **2016**, *23*, 22–30.

13. Liu, H.T.; Li, X.; Wan, Y.Q.; Liu, Z.B.; Zhou, L.; Che, S.Q. Formation conditions and exploration and development potential of continental shale gas: A case of Dongyuemiao Member of the Jurassic in north Fuling area, eastern Sichuan Basin. *Mar. Orig. Pet. Geol.* **2020**, *25*, 148–154.
14. Iyare, U.C.; Blake, O.O.; Ramsook, R. Brittleness evaluation of Naparima Hill mudstones. *J. Pet. Sci. Eng.* **2021**, *196*, 107737. [CrossRef]
15. Li, W.; Liu, J.S.; Zeng, J.; Leong, Y.K.; Elsworth, D.; Tian, J.W.; Li, L. A fully coupled multidomain and multiphysics model for evaluation of shale gas extraction. *Fuel* **2020**, *278*, 118214. [CrossRef]
16. Liu, B.; Yan, M.; Sun, X.D.; Bai, Y.F.; Bai, L.H.; Fu, X.F. Microscopic and Fractal Characterization of Organic Matter within Lacustrine Shale Reservoirs in the First Member of Cretaceous Qingshankou Formation, Songliao Basin, Northeast China. *J. Earth Sci.* **2020**, *31*, 1241–1251. [CrossRef]
17. Iqbal, M.A.; Rezaee, R.L.C.; Pejcic, B.; Smith, G. Integrated sedimentary and high-resolution mineralogical characterisation of Ordovician shale from Canning Basin, Western Australia: Implications for facies heterogeneity evaluation. *J. Pet. Sci. Eng.* **2022**, *208*, 109347. [CrossRef]
18. Liu, Y.J.; Lai, F.Q.; Zhang, H.J.; Tan, Z.J.; Wang, Y.F.; Zhao, X.T.; Tan, X.F. A novel mineral composition inversion method of deep shale gas reservoir in Western Chongqing. *J. Pet. Sci. Eng.* **2021**, *202*, 108528.
19. Wang, R.Y.; Ding, W.L.; Zhang, Y.Q.; Wang, Z.; Wang, X.H.; He, J.H.; Zeng, W.T.; Dai, P. Analysis of developmental characteristics and dominant factors of fractures in Lower Cambrian marine shale reservoirs: A case study of Niutitang formation in Cen'gong block, southern China. *J. Pet. Sci. Eng.* **2016**, *138*, 31–49. [CrossRef]
20. Wang, R.Y.; Hu, Z.Q.; Long, S.X.; Du, W.; Wu, J.; Wu, Z.H.; Nie, H.K.; Wang, P.W.; Sun, C.X.; Zhao, J.H. Reservoir characteritics and evolution mechanisms of the Upper Ordovician Wufeng-Lower Silurian Longmaxi shale, Sichuan Basin. *Oil Gas Geol.* **2022**, *43*, 353–364.
21. Wang, R.Y.; Hu, Z.Q.; Zhou, T.; Bao, H.Y.; Wu, J.; Du, W.; He, J.H.; Wang, P.W.; Chen, Q. Characteristics of fractures and their significance for reservoirs in Wufeng-Longmaxi shale, Sichuan Basin and its periphery. *Oil Gas Geol.* **2021**, *42*, 1295–1306.
22. Li, B.K.; Nie, X.; Cai, J.C.; Zhou, X.Q.; Wang, C.C.; Han, D.L. U-Net model for multi-component digital rock modeling of shales based on CT and QEMSCAN images. *J. Pet. Sci. Eng.* **2022**, *216*, 110734. [CrossRef]
23. Liu, B.; Gao, Y.F.; Liu, K.Q.; Liu, J.Z.; Ostadhassan, M.; Wu, T.; Li, X.L. Pore structure and adsorption hysteresis of the middle Jurassic Xishanyao shale formation in the Southern Junggar Basin, northwest China. *Energy Explor. Exploit.* **2021**, *39*, 761–778. [CrossRef]
24. Liu, Z.B.; Liu, G.X.; Hu, Z.G.; Feng, D.J.; Zhu, T.; Bian, R.K.; Jiang, T.; Jin, Z.G. Lithofacies types and assemblage features of continental shale strata and their significance for shale gas exploration: A case study of the Middle and Lower Jurassic strata in the Sichuan Basin. *Nat. Gas Ind. B* **2019**, *39*, 10–21.
25. Liu, J.S.; Ding, W.L.; Xiao, Z.K.; Dai, J.S. Advances in comprehensive characterization and prediction of reservoir fractures. *Prog. Phys.* **2019**, *34*, 2283–2300.
26. Wei, Y.; Nie, X.; Jin, L.D.; Zhang, C.; Zhang, C.M.; Zhang, Z.S. Investigation of sensitivity of shale elastic properties to rock components based on a digital core technology and finite element method. *Arab. J. Geo-Sci.* **2018**, *11*, 1–14. [CrossRef]
27. Ding, W.L.; Zhu, D.W.; Cai, J.J.; Gong, M.L.; Chen, F.Y. Analysis of the developmental characteristics and major regulating factors of fractures in marine–continental transitional shale-gas reservoirs: A case study of the Carboniferous–Permian strata in the southeastern Ordos Basin, central China. *Mar. Pet. Geol.* **2013**, *45*, 121–133. [CrossRef]
28. Ma, C.F.; Dong, C.M.; Lin, C.Y.; Elsworth, D.; Luan, G.; Sun, X.L.; Liu, X.C. Corrigendum to "Influencing factors and fracability of lacustrine shale oil reservoirs". *Mar. Pet. Geol.* **2021**, *124*, 104861. [CrossRef]
29. Guo, X.S.; Zhao, Y.Q.; Zhang, W.T.; Li, Y.P.; Wei, X.F.; Shen, B.J. Accumulation conditions and controlling factors for the enrichment of shale oil and gas in the Jurassic Qianfoya Formation, Yuanba Area, Sichuan Basin. *Pet. Geol. Exp.* **2021**, *43*, 749–757.
30. Hu, Z.Q.; Wang, R.Y.; Liu, Z.B.; Liu, G.X.; Feng, W.J.; Yang, Z.H.; Wang, P.W. Source-reservoir characteristics and coupling evaluations for the Lower Jurassic lacustrine shale gas reservoir in the Sichuan Basin. *Geosci. Front.* **2021**, *28*, 261–272.
31. Wang, R.Y.; Gong, D.J.; Ding, W.L.; Leng, J.G.; Yin, S.; Wang, X.H.; Sun, Y.X. Brittleness evaluation of the Lower Cambrian Niutitang shale in the Upper Yangtze region: A case study in the Cengong Block, Guizhou Province. *Geosci. Front.* **2016**, *23*, 87–95.
32. Zhang, J.J.; Salad, H.O.; Shi, S.M.; Cao, Y.F.; Sun, J.Y. Indicators for identification of lacustrine sandstones of sandy debris-flow origin: A case study of Es1 Member, Palaeogene Shahejie Formation, Nanpu Sag, Bohai Bay Basin, China. *Geol. J.* **2022**, *57*, 3178–3198. [CrossRef]
33. Cao, D.S.; Zeng, L.B.; Lv, W.Y.; Xu, X.; Tian, H. Progress in brittleness evaluation and prediction methods in unconventional reservoirs. *Pet. Sci. Bull.* **2021**, *6*, 31–45.
34. He, J.H.; Li, Y.; Deng, H.C.; Tang, J.M.; Wang, Y.Y. Quantitative evaluation and influencing factors analysis of the brittleness of deep shale reservoir based on multiple rock mechanics experiments. *Nat. Gas Geosci.* **2022**, *33*, 1102–1116.
35. Wang, X.Y.; Jin, Z.K.; Guo, Q.H.; Wang, J.Y.; Ren, Y.L.; Wang, L.; Wang, Z.F. Genesis of Calcite in Nonmarine Shale of the Lower Jurassic Da'anzhai Member, Northeastern Sichuan. *Acta Sedimentol. Sin.* **2021**, *39*, 704–712.
36. Liu, J.S.; Ding, W.L.; Yang, H.M.; Dai, P.; Wu, Z.H.; Zhang, G.J. Natural Fractures and Rock Mechanical Stratigraphy Evaluation in theHuaqingarea, Ordos Basin: A Quantitative Analysis Based on Numerical Simulation. *J. Earth Sci.* **2022**, 1–19. Available online: http://kns.cnki.net/kcms/detail/42.1874.P.20220711.0942.004.html (accessed on 1 February 2023).

37. Ding, W.L.; Zeng, W.T.; Wang, R.Y.; Jiu, K.; Wang, Z.; Sun, Y.X.; Wang, X.H. Method and application of tectonic stress field simulation and fracture distribution prediction in shale reservoir. *Geosci. Front.* **2016**, *23*, 63–74.
38. Huang, Y.Y.; Wang, G.W.; Han, Z.Y. Micro resistivity imaging logging—The "perspective eye" of petroleum explorers. *Pet. Knowl.* **2022**, *1*, 14–19.

Disclaimer/Publisher's Note: The statements, opinions and data contained in all publications are solely those of the individual author(s) and contributor(s) and not of MDPI and/or the editor(s). MDPI and/or the editor(s) disclaim responsibility for any injury to people or property resulting from any ideas, methods, instructions or products referred to in the content.